Available online at www.sciencedirect.com
ScienceDirect
Cement and Concrete Research 37 (2007) 438–454
Cement and Concrete Research

Water vapour sorption experiments on hardened cementitious materials. Part II: Essential tool for assessment of transport properties and for durability prediction

Véronique Baroghel-Bouny *

Laboratoire Central des Ponts et Chaussées, 58 Bd Lefebvre, F-75732 Paris Cedex 15, France

Received 7 September 2006; accepted 17 November 2006

Abstract

This paper forms the second part of a series. In this second part, transport properties are theoretically and experimentally studied on various hardened cementitious materials, in order to evaluate the influence of some parameters (degree of saturation, mix-composition, …). Water vapour and moisture diffusion coefficients, as well as liquid water or gas permeability, as a function of the degree of saturation can be assessed from water vapour sorption experiments along with a complementary test, a numerical model and/or analytical formulas. Here, the analysis focuses in particular on the meaning of the various coefficients obtained by different methods. The results point out that, owing to the complex phenomena that take place during drying–wetting processes and to their moisture history dependency, inadequacy can arise between the diffusion coefficients involved in the theoretical description and those actually measured. Moreover, the concept of intrinsic permeability, independent of the permeating fluid, does not seem relevant for cementitious materials when liquid water is regarded, except maybe for highly permeable ones.

Keywords: (B) Degree of saturation; (C) Moisture transport–diffusion coefficient–permeability; (E) Cementitious material

1. Introduction

All of the possible deterioration mechanisms, even endogenous, that may affect the durability of reinforced concrete (RC) structures involve either gaseous or liquid (e.g. ionic) transport processes. As far as reinforcement corrosion is concerned, the transport of carbon dioxide gas, oxygen and chloride ions can be involved, in addition to that of moisture. As regards alkali–silica reaction, alkaline, calcium and silicate ions are involved. These processes (particularly their rate) and their couplings are controlled, not only by the "pure" transport properties of the material (reflecting the pore structure), but also by the fluid-matrix interactions (water sorption, chloride binding, …) owing to the high reactivity of the solid matrix of concrete to water and to various species. Both types of parameters will hence play a central role in the quantification and the prediction of durability of RC structures.

It has been shown in the first part of the paper series [1] that water vapour desorption and adsorption experiments provide:

- the "equilibrium" moisture properties, more exactly the so-called water vapour desorption and adsorption isotherms (WVSIs), which plot the equilibrium mass water content of the (hardened) material *vs.* relative humidity (RH), at a constant temperature,
- the pore structure characteristics of the (hardened) material,

and thus allow an accurate analysis of the hygral behaviour of hardened cementitious materials and its relation to pore structure.

Water vapour desorption and adsorption experiments can also provide transport properties (permeability and diffusion coefficients). For example, the *apparent* moisture diffusion coefficient can be directly deduced with some assumptions (see Section 3.2) from the analysis of the plots which give the relative mass loss *vs*. time (so-called kinetics) associated with each RH step performed to assess WVSIs by means of the

* Tel.: + 33 1 40 43 51 32; fax: + 33 1 40 43 54 98.
E-mail address: baroghel@lcpc.fr.

0008-8846/$ - see front matter © 2006 Elsevier Ltd. All rights reserved.
doi:10.1016/j.cemconres.2006.11.017

saturated salt solution method described in [1]. The *apparent* moisture diffusion coefficient is the global and moisture-dependent transport coefficient involved in the non-linear diffusion-type equation (Fick's second law), which governs moisture transport in partially saturated and non-steady state conditions. The component associated with water vapour of this *apparent* moisture diffusion coefficient, according to the usual description of isothermal moisture transport (which assumes in particular a constant gas pressure), can also be assessed from the WVSI (*integral moisture capacity*) or its slope (*differential moisture capacity*) and by performing a "cup test" (see Section 3.3). In addition, the relative permeability to liquid water (see Section 4.4) and to gas (see Section 5.3) can be deduced from WVSIs thanks to analytical formulas proposed in the literature.

The present paper is devoted to the assessment of transport properties of hardened cementitious materials. Various cement pastes and concretes are tested. The results obtained by means of different methods, in particular those previously described, which involve water vapour sorption data, are compared and discussed. The effect of the degree of liquid water saturation is studied. In addition, the similarities and the differences between the different materials are investigated, in particular the influence of mix-parameters such as the water-to-cement ratio (W/C). Moreover, the analysis focuses on the meaning of the coefficients obtained by the various methods. The possibility to assess intrinsic data is investigated. It is indeed of primary importance to be able to assess transport properties by means of well-defined test methods, and to correctly understand the meaning of the parameters thus quantified, in order for example to use them as input data in physically and chemically based predictive models.

2. Materials tested

Several cement pastes (referenced CP, CN, CO, and CH) and concretes (referenced BO-AF, BO-SN, BO, BH, M25, B80-S, and B30-A) with:

- various type-I OPCs (CEM I- 52.5, according to the EN 197-1 European standard),
- a broad range of water-to-cement ratios: W/C ranges from 0.20 to 0.84,
- possible incorporation of silica fume (SF): SF/C ranges from 0 to 0.10,

have been studied in laboratory.

The mixture proportions of the concretes and the cement pastes are summarized in Tables 1 and 2 respectively. The series numbers defined in [1] are reported in the tables. For a given series, the constituents (cement, silica fume, and aggregates) are the same. The aggregates were dried before mixing. The mineralogical composition, calculated by Bogue's formula from the chemical composition, and the Blaine fineness of the cements used are given in Table 3. Some of the mixtures (CH, BH, and B80-S) are high performance (HP) materials: they are prepared with a low W/C, with silica fume, and with superplasticizer. The silica fume was added as dry powder. The chemical composition of the silica fumes used and their BET specific surface area (measured by nitrogen adsorption) are given in Table 4. Note that the mixture B80-S has been used for the building of a bridge in France ("Sens Bridge"): the sorption experiments (see [1]) were therefore performed on specimens prepared from cores extracted from the inner zone of this bridge. The concretes BO-AF and BO-SN (series 2*) are not reported in Table 1, since their constituents and mix-composition are similar to those of BO (series 2). Only the cement (see Table 3) and the initial water content are slightly different. The respective W/C are 0.49 and 0.44.

Table 1
Mix-composition and compressive strength of the concretes

Series (cement) reference	2		3		4
Material reference	BO	BH	M25	B80-S	B30-A
Gravel (G) content (in kg m^{-3})	1192	1265	1007	980	1075
(min/max grain size in mm)	(4/20)	(4/20)	(5/20)	(6/14)	(4/20)
Sand (S) content (in kg m^{-3})	744	652	899	790	764
(min/max grain size in mm)	(0/5)	(0/5)	(0/5)	(0/4)	(0/4)
Cement (C) content (in kg m^{-3})	353	421	230	420	350
Silica fume (SF) content (in kg m^{-3})		42.1		35	
Water (W) content (in kg m^{-3})	152	112.3	193	147	175
Superplasticizer content (in kg m^{-3})		7.59		7.28	
Water-to-cement ratio (W/C)	0.43	0.27	0.84	0.35	0.50
Water-to-binder ratio (W/B)		0.24	0.84	0.32	0.50
Silica fume to cement ratio (SF/C)		0.10		0.08	
Gravel-to-sand ratio (G/S)	1.6	1.9	1.1	1.2	1.4
28-day cylinder average compressive strength (in MPa)	49.4	115.5	25.1	85.3	37.5

3. Water vapour and moisture diffusion coefficients — definitions, measurement, experimental results and interpretation

3.1. Influencing parameters

3.1.1. Introduction

Diffusion coefficients are theoretically and experimentally studied in Section 3, in order to clarify the meaning of the coefficients quantified by various techniques and to investigate the influence of some parameters.

The physical (and possibly chemical) processes involved in moisture diffusion may vary with the test method used to assess a parameter which characterizes this transport. Therefore, various methods may yield theoretically different transport coefficients, whose physical meaning will mainly depend on the saturation state of the test specimen, the nature of the gradient (driving force), the scale at which the measurement is performed, and the test conditions (steady or non-steady-state regime). Here, the problem is more complicated than in the case of ionic diffusion for example, since the presence of both liquid and vapour phases has to be taken into account.

3.1.2. The saturation state

The saturation state is a first parameter that allows the methods to be distinguished. During a diffusion process in

Table 2
Mix-composition of the cement pastes

Series (cement) reference	2			
Material reference	CP	CN	CO	CH
Water-to-cement ratio (W/C)	0.60	0.45	0.35	0.20
Water-to-binder ratio (W/B)	0.60	0.45	0.35	0.18
Silica fume to cement ratio (SF/C)				0.10

saturated conditions, the pore network of the material is filled with the liquid phase. As regards water, this is the case when the (air-void free) test specimen is in contact with a liquid reservoir or when it is in equilibrium with an environment whose vapour pressure is greater or equal to the equilibrium pressure calculated with respect to the biggest pores of the material through the Kelvin equation (see Eq. (11) in Section 3.4.1). Moisture diffusion in non-saturated conditions occurs when the pore volume is only partially filled with the liquid phase. This is the case when the test specimen is (locally) in equilibrium with an environmental water vapour pressure lower than the saturating vapour pressure at the considered temperature. As described in [1], in this case the non-saturated-pore walls are covered with an adsorbed water layer, whereas the empty cores are filled with a dry air and water vapour gas mixture. The moisture transport mechanism then involves both the gas and the liquid phases.

3.1.3. The nature of the gradient (driving force)

Two types of water diffusion process are usually distinguished, depending on the presence of a water content gradient ("chemical" gradient). As regards self-diffusion of water, the test methods consist in monitoring the random movements of a population of (isotopically, magnetically, …) marked individuals, but chemically indiscernible from the non-marked individuals (see Section 3.2.3 and [2]). At the macroscale, the water content is the same at any location in the test specimen (saturated conditions). As far as "chemical" diffusion is concerned, the water movements result from a water content gradient. Various types of boundary conditions can yield such a gradient: for example an RH imbalance between the two sides of a test specimen (see Section 3.3).

3.1.4. The measurement scale

Moisture diffusion can be considered at both the macroscopic and microscopic scales. Measurement at the microscopic scale will quantify the diffusion process only at the pore scale. In the extreme case of a method which allows a measurement within a single saturated pore, sufficiently large so that the effect of the molecule-wall interaction on water mobility is negligible, one should find the self-diffusion coefficient of free water (more exactly of the pore solution) [2]. In the case of macroscopic measurement, the parameter that characterizes diffusion is measured at a length scale equal or higher than the size of a Representative Elementary Volume (REV) of the porous medium. The result will then include the porosity and the geometry of the pore network. In the present paper, for practical relevance, the moisture transport will be described and the transport properties will be measured only at the macroscale.

3.1.5. The steady or non-steady state conditions

Tests can be performed under steady or non-steady-state conditions. Under steady-state conditions (constant flux density), Fick's first law is generally used to directly assess an *effective* diffusion coefficient (see Section 3.3). Under non-steady-state conditions (flux density variable as a function of time), it is necessary to solve Fick's second law, in order to assess an *apparent* diffusion coefficient (see Section 3.2).

3.2. 1-D isothermal moisture transport at the macroscale in the partially saturated pore network under non-steady-state conditions — apparent moisture diffusion coefficient

3.2.1. Usual approach and methods of assessment of the apparent moisture diffusion coefficient D_a

Under non-steady-state conditions, in cementitious materials assumed as a porous medium partially saturated by the liquid phase, the isothermal moisture transport is usually described at the macroscopic scale by using Fick's second law (also known in this case as Richard's equation). In a 1-D scheme, the various formulas proposed in the literature (see for example [3,4,5,6,7,8,9,10]) yield writing a single non-linear diffusion-type equation (Eq. (1)), which governs the evolution of the degree of liquid water saturation S_l:

$$\frac{\partial S_l}{\partial t} - \frac{\partial}{\partial x}\left(D_a(S_l)\frac{\partial S_l}{\partial x}\right) = 0 \tag{1}$$

where $D_a(S_l)$ denotes the so-called *apparent moisture diffusion coefficient*.

Table 3
Mineralogical composition and Blaine fineness of the cements

Series	Content (%)								Blaine fineness ($m^2\ kg^{-1}$)
	C_3S	C_2S	C_3A	C_4AF	Gypsum	$CaCO_3$	Free CaO	Alkalis	
2	57.3	24.0	3.0	7.6	4.4	1.8	0.53	Na_2O=0.43 K_2O=0.43	317
2*	63.9	15.0	3.8	5.4	4.8	2.7	0.99	Na_2O=0.19 K_2O=0.26	320
3	57.6	17.8	2.2	12.6	6.2	2.0	0.71	Na_2O=0.12 K_2O=0.30	355
4	59.1	14.5	9.1	9.0			0.97	Na_2Oeq.=0.81	353

Table 4
Chemical composition and BET specific surface area (measured by nitrogen adsorption) of the silica fumes

Series	Content (%)							S_sBET (N_2) ($m^2.g^{-1}$)
	SiO_2	Al_2O_3	Fe_2O_3	MgO	MnO	CaO	Alkalis	
2	87.0	0.27	0.67	1.56	0.07	0.37	Na_2O=0.70 K_2O=2.35	17.6
3	96.0	0.18	0.55	0.65	0.13	0.22	Na_2O=0.25 K_2O=1.05	16.2

A review of the literature shows that various methods are used to assess in a more or less direct way this global and moisture-dependent transport coefficient. The analysis of gamma-ray, X-ray, neutron or NMR moisture profiles associated with drying or wetting experiments under non-steady-state regime and well-defined initial and boundary conditions by using Boltzmann's transform method is often applied (see for example [4,6,7,8,9]). In this paper, $D_a(S_l)$ will be assessed under non-saturated and non-steady-state conditions from sorption kinetics (see Section 3.2.2).

3.2.2. Apparent moisture diffusion coefficient D_a — method of assessment from sorption kinetics under non-steady-state conditions

The test method consists in monitoring the relative loss or increase in mass of a specimen (sorption kinetics), during a RH step carried out in order to assess WVSIs by means of the saturated salt solution method (see [1,11]). As small RH steps are imposed during the experiment, it can be assumed that $D_a(S_l)$=constant=D_a within each RH interval. In this case, Fick's second law reads (Eq. (2)):

$$\frac{\partial S_l}{\partial t} = D_a \cdot \frac{\partial^2 S_l}{\partial x^2} \tag{2}$$

This linear differential equation can be solved by applying Crank's method [12]: within each RH interval, the *apparent* moisture diffusion coefficient is given by Eq. (3):

$$D_a = A(\alpha) \cdot \frac{e^2}{t_\alpha} \tag{3}$$

where t_α denotes the time at which $\Delta M/\Delta M(t_\infty)=\alpha$ (e.g. $\alpha=0.5$) with ΔM the relative mass variation (in %), e is the specimen thickness, and $A(\alpha)$ is a mathematical series.

A detailed description of the method, assumptions and computation is given in [8,11]. D_a is thus assessed by fitting the values calculated with the analytical formula, or with a simplified expression of $A(\alpha)$, on the experimental relative mass variations *vs*. drying time (see the example displayed in Fig. 1). Note that such fitting can allow the relative mass variation values at "equilibrium" states to be checked (by comparison between the experimental "equilibrium" value and the value calculated at a longer exposure time).

3.2.3. Apparent moisture diffusion coefficient D_a — experimental results, discussion and comparison with effective tritiated water diffusion coefficient

In this section, the experimental results obtained on various materials with respect to the *apparent* diffusion coefficient D_a are presented and analysed.

For a given material (e.g. hcp CH, see Fig. 2), when the D_a data are plotted *vs*. RH, a significant hysteresis effect is observed between the results obtained in desorption and adsorption regimes (see Fig. 2a). But when the data are plotted *vs*. the degree of liquid water saturation S_l, the hysteresis effect disappears and similar results are displayed in desorption and in adsorption until the high saturation range (see Fig. 2b). This confirms the major role of the degree of saturation and can contribute to explain the hysteretical behaviour of cementitious materials.

The results obtained in the adsorption regime for various hcps and concretes from series 2, 2* and 3 (3 OPCs CEM I-52.5; W/C ranging from 0.20 to 0.84; SF/C ranging from 0 to 0.10) are plotted *vs*. RH in Fig. 3. Similar trends over the whole range are observed on the available data for the various materials tested. If the borderline pointed out on water vapour adsorption isotherms (WVAIs) in [1] (RH=63.2%) is reported in the figure, it can be seen that:

- for RH<63.2% (surface multilayer adsorption range), only a slight influence of RH is recorded,
- at RH=63.2%, a change of regime is observed and D_a decreases significantly, from $1–10 \cdot 10^{-12}$ m^2 s^{-1} below the borderline to $0.01–0.1 \cdot 10^{-12}$ m^2 s^{-1} above the borderline (bulk capillary absorption range).

The results are thus in agreement with those provided through the analysis of the WVAIs (see [1]). The mix-composition or the test temperature effects can also be investigated (see Fig. 3): D_a increases when W/C or the temperature increases (see the results obtained for BO-AF at $T=44\pm0.1$ °C).

For the various materials tested (hcps and concretes from series 2, 2* and 3 with 3 OPCs CEM I-52.5; W/C ranging from 0.20 to 0.84; SF/C ranging from 0 to 0.10), the D_a results plotted *vs*. the degree of liquid water saturation S_l (see Fig. 4) exhibit roughly the same trends over the whole range, regardless

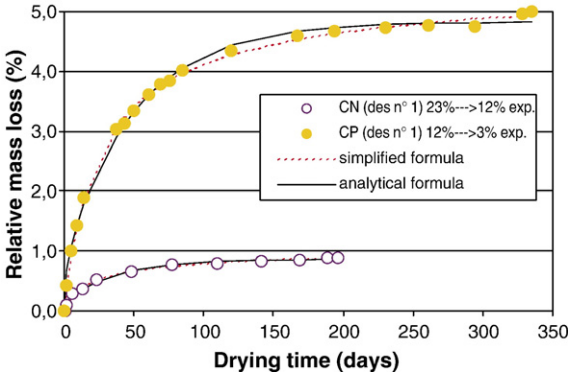

Fig. 1. Fitting of the values calculated with the analytical formula or a simplified formula of $A(\alpha)$ on experimental relative mass losses *vs*. drying time (desorption kinetics) obtained on hcps CN (W/C=0.45) and CP (W/C=0.60) (series 2).

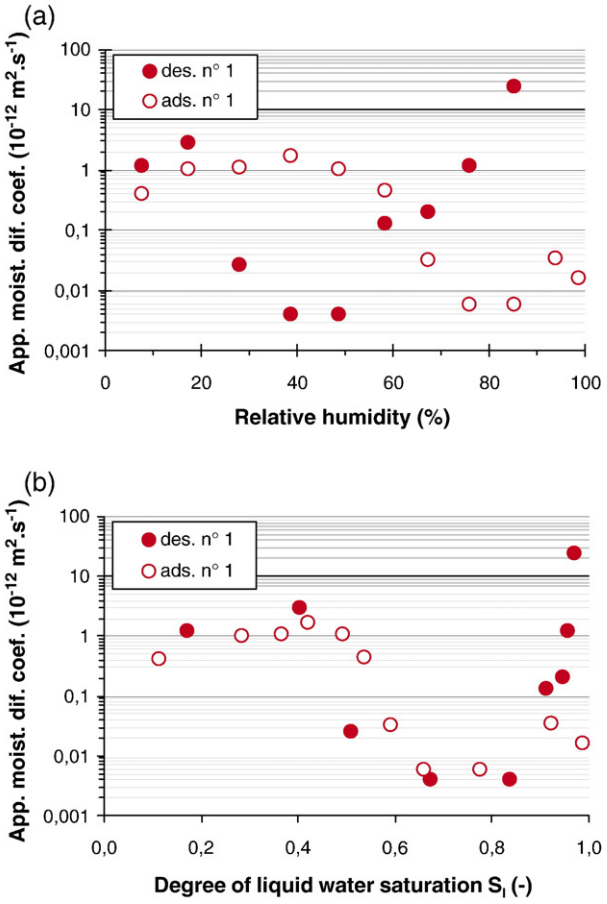

Fig. 2. *Apparent* moisture diffusion coefficient D_a assessed from sorption kinetics (under non-steady-state conditions), on HP hcp CH (series 2; W/C=0.20; SF/C=0.10). a) *vs.* RH; b) *vs.* degree of liquid water saturation S_l.

of the mixture (in particular when CH is disregarded) and of the (desorption or adsorption) regime. However, an obvious scatter of the results is observed, as often reported in the literature [10,13]. Large variations are observed as a function of S_l. Most of the values lie within the range: $10^{-14} \le D_a(S_l) \le 10^{-11}$ m^2 s^{-1}. Roughly speaking, when S_l increases from 0 to around 0.50, D_a decreases. A minimum appears in the mid S_l range, in particular in the case of desorption (see Fig. 4), in agreement with the literature (see e.g. the experimental results displayed in [6,7,10]), and which is symptomatic of a (liquid phase) percolation phenomenon in porous materials. However, the exact location of this minimum seems to depend on the material. More precisely, in the case of CH, D_a is particularly small and the liquid phase continuity will take place at a higher degree of saturation (between 0.60 and 0.80) compared to the other materials. This result is consistent with the pore structure characteristics of this material (see [1,11]): in this material, the transport is controlled by the HD, i.e. high-density, C–S–H pore network (since the hcp CH has been found mainly composed of HD C–S–H, according to [1]). These findings are also consistent with the numerical computations reported in [14], as regards the relative importance of the various driving forces of moisture transport. When S_l increases beyond the minimum, D_a seems to increase, although less data are available within this range. The variations of D_a *vs.* S_l in the very low and very high ranges seem to greatly depend on the adsorption/desorption regime (see e.g. the CN and CH results, in the low and high ranges respectively).

Values at $S_l=1$ are plotted in Fig. 4 for CH, CO and CN. These values have been measured in saturated and steady-state conditions at the macroscopic scale by means of tritiated water (i.e. effective tritiated water diffusion coefficients). They are drawn from [2]. The test was performed by using a diffusion cell where the specimen is sandwiched between two compartments. The upstream compartment is filled with a saturated lime solution containing tritiated water and the downstream compartment with non-radioactive lime water. Negligible chemical interaction is usually assumed between tritiated water and cement matrix. The test method consists in the monitoring of the increase in the radioactivity in the downstream compartment, as described in [2]. The diffusion coefficient is then calculated within the steady-state range by using Fick's first law. Fig. 4 highlights that there is a good consistence between this coefficient and the other plots obtained within the high S_l range for the same material, more precisely, the desorption data available for CN and CO, and an average value between desorption and adsorption values for CH. Note that a very good agreement is observed between the *effective* tritiated water diffusion coefficients reported here and those given in [15]. Note in addition that all of these values are drastically lower than the tritiated water diffusion coefficient in bulk water ($D_{0(HTO)}=1–2.5\cdot10^{-9}$ m^2 s^{-1}, as deduced from the literature). Since the transport is controlled by the HD C–S–H pore network in CH, as previously mentioned, it can be assumed that the *effective* tritiated water diffusion coefficient measured on this material ($D_{e(HTO)}=0.12\cdot10^{-9}$ m^2 s^{-1}) is more or less the intrinsic diffusion coefficient of the HD C–S–H.

The experimental results displayed in Fig. 4 underline the complex liquid/vapour mechanisms (transport along with interactions), which take place in the pore system during the experiments, highlighting again the importance of the moisture

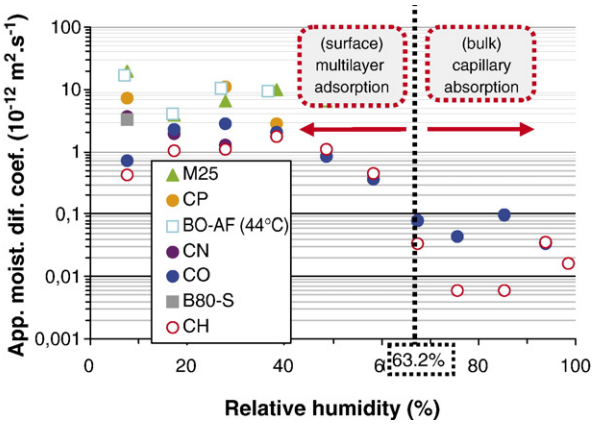

Fig. 3. *Apparent* moisture diffusion coefficient D_a *vs.* RH, assessed from adsorption kinetics (under non-steady-state conditions), on various hcps and concretes (series 2, 2* and 3; $0.20 \le W/C \le 0.84$; $0 \le SF/C \le 0.10$). For some mixtures (M25, CP, BO-AF, CN, and B80-S), D_a is not yet available within the whole RH range.

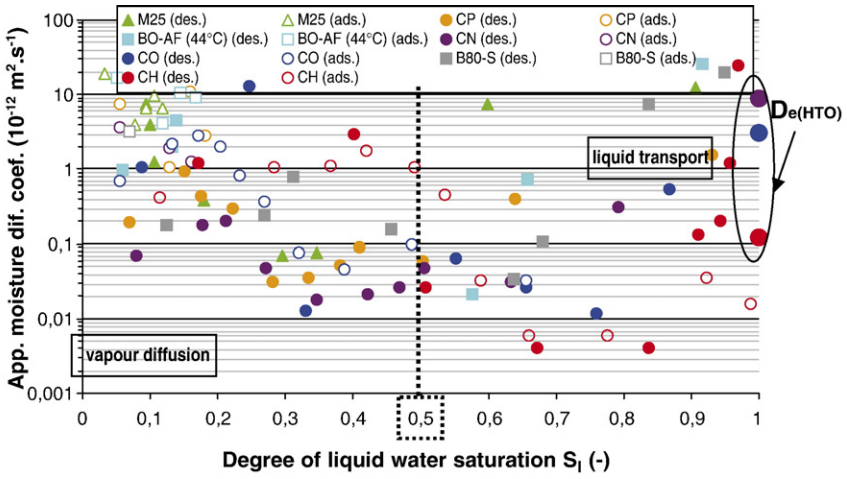

Fig. 4. *Apparent* moisture diffusion coefficient D_a *vs.* degree of liquid water saturation S_l, assessed from sorption kinetics (under non-steady-state conditions), on various hcps and concretes (series 2, 2* and 3; $0.20 \le W/C \le 0.84$; $0 \le SF/C \le 0.10$). Comparison with *effective* tritiated water diffusion coefficient $D_{e(HTO)}$ (under steady-state conditions) for hcps CH, CO and CN [2].

history of the test specimen and in particular of the initial moisture state at the starting time of the experiments.

Eq. (1) is usually introduced by invoking two main assumptions. First, the water vapour transport is governed by a pure diffusion process (i.e. the advective gas flow is negligible with respect to the diffusive flow of the vapour phase). Secondly, the total gas (dry air+water vapour) pressure remains (almost) constantly equal to the outer atmospheric pressure during the transport time scale. With these two assumptions (and by using the ideal mixture law and Kelvin equation), Mainguy [16], on the basis of the works by Philip and de Vries [17,18] and by more recent researchers in this field (e.g. [4,19]), has shown that the moisture diffusivity $D_a(S_l)$ is expressed as the sum of two components (see Eq. (4)):

$$D_a(S_l) = D_l(S_l) + D_v(S_l) \tag{4}$$

where:

$$D_l(S_l) = -\frac{dp_c}{dS_l} \cdot \frac{K_l}{\Phi \eta_l} k_{rl}(S_l) \quad \text{and}$$

$$D_v(S_l) = -\frac{dp_c}{dS_l} \cdot \left(\frac{M}{\rho_l RT}\right)^2 \cdot D_{v0} \cdot f(S_l, \phi) \cdot \frac{p_{vs}}{\Phi} \times \exp\left(\frac{M}{\rho_l RT} p_c(S_l)\right) \tag{5}$$

Eqs. (4) and (5) indicate that, in addition to moisture–solid interactions (sorption), the global and moisture-dependent transport coefficient $D_a(S_l)$ implicitly includes two moisture transport modes, which are coupled and which act simultaneously with the assumption of (almost) constant gas pressure:

- The Darcian (advective) transport of liquid water governed by the permeability of the non-saturated medium $K_l k_{rl}(S_l)$ (see Section 4.1). The component $D_l(S_l)$ is associated with this mode, where $k_{rl}(S_l)$ is the relative permeability to liquid water ($k_{rl} \le 1$), K_l the "intrinsic" liquid water permeability (i.e. the permeability of the fully saturated material) independent of the degree of liquid water saturation S_l and theoretically independent of the permeating fluid, p_c the capillary pressure, Φ the bulk porosity accessible to water of the material, and η_l the dynamic viscosity of liquid water (assumed to be an incompressible fluid).
- The Fickian (diffusive) transport of water vapour governed by the *effective* water vapour diffusion coefficient in the porous medium $D_{ve}(S_l) = D_{v0} \cdot f(S_l, \Phi)$, where D_{v0} is the free (out of the porous medium) water vapour diffusion coefficient in the air ($D_{v0} = 2.47 \cdot 10^{-5}$ m^2 s^{-1} between $T = 20$ and 25 °C), and $f(S_l, \Phi)$ is the so-called resistance factor, which accounts for both the tortuosity effects and the reduction of space offered to gas diffusion in a partially saturated porous medium, compared to free diffusion in the air (see Section 3.3). The component $D_v(S_l)$ is associated with this mode (along with sorption phenomena), where T is the absolute temperature, R the universal gas constant ($R = 8.3144$ J mol^{-1} K^{-1}), M the molar mass of water ($M = 18 \cdot 10^{-3}$ kg mol^{-1}), ρ_l the liquid water mass density, and p_{vs} the saturating water vapour pressure at the considered temperature T (e.g. $p_{vs} = 2338.54$ Pa at $T = 20$ °C and $p_{vs} = 2810.06$ Pa at $T = 23$ °C, when $p_g = p_{atm}$).

Depending on the considered material and on its saturation state, one or the other process can be prominent. In the general case, vapour diffusion is prominent within the low S_l range, whereas liquid transport is prominent within the high S_l range, for the same reasons that explain the evolutions of the relative permeabilities to liquid water and to gas *vs.* S_l (see Fig. 9 in Sections 4 and 5). However, in the case of water vapour, the problem is more complex (than in the case of oxygen gas), as with the previously mentioned assumptions, its transport is coupled with that of liquid water. The variations of D_a *vs.* S_l observed in Fig. 4 should therefore be explained by the variations observed on D_{ve} or D_v within the S_l range [0; 0.50] (see Figs. 6 and 7 in Sections 3.3 and 3.4 respectively) and on k_{rl}

within the S_l range [0.50; 1] (see Fig. 9 in Section 4.4) as a function of S_l. Since both coefficients are reduced within the mid S_l range (as it will be detailed later), a minimum can be deduced for the global transport and therefore for the D_a plot. This minimum therefore results from the transition from transport dominated by Darcian flow (at high RHs) to vapour diffusion (at low RHs), and from the fact that vapour diffusion increases as RH decreases, because there are fewer pores blocked by the disconnected liquid phase.

It can be concluded that it is more relevant for an improved understanding of moisture transport processes, and in particular to study the relative contribution of each transport mode as a function of the material pore structure and of the degree of saturation, to assess $D_{ve}(S_l)$ (or $D_v(S_l)$) and $K_l k_{rl}(S_l)$ separately, instead of measuring a global coefficient. $D_{ve}(S_l)$ (or $D_v(S_l)$) can be assessed from the cup test (see Section 3.3). As far as the liquid water permeability is concerned, its assessment will be discussed in Section 4.

3.3. 1-D isothermal diffusive transport at the macroscale of water vapour in the gaseous phase of the pore network under steady-state conditions — effective water vapour diffusion coefficient

3.3.1. Equations and definitions

When the water vapour concentration is higher outside a test specimen than inside, the gradient forces water to penetrate into the porous material. Under steady-state conditions, such an isothermal diffusive transport of water vapour in the partially saturated pore network of the material is governed by Fick's first law. The water vapour mass flux density J_v through the surface of the porous material (in kg m^{-2} s^{-1}) is then given in a 1-D scheme along a Ox-axis by Eq. (6):

$$J_v = -D_{ve} \cdot \frac{\partial c_v}{\partial x} \tag{6}$$

where $c_v(x,t)$ is the water vapour concentration (i.e. absolute humidity) in the gaseous phase of the pore network at a distance x from the surface exposed and at time t (in kg m^{-3}).

By taking into account the relationship between c_v and the water vapour partial pressure p_v, Eq. (6) reads (see Eq. (7)):

$$J_v = -\delta \cdot \frac{\partial p_v}{\partial x} = -D_{ve} \cdot \frac{M}{RT} \cdot \frac{\partial p_v}{\partial x} \tag{7}$$

where δ (expressed in kg m^{-1} s^{-1} Pa^{-1}) is usually called "*permeability*" *to water vapour* (although this coefficient is, by definition, associated with a diffusion process).

The "permeability" to water vapour of a porous material at a given temperature is a property often used in the building field, in order to describe the hygrothermal behaviour of building walls and to study their susceptibility to condensation (see for example [20]).

Hence, when a cementitious test specimen (thickness e, in m, and e.g. initial internal relative humidity h_2) is sandwiched between two environments at same temperature T, but where prevail different relative humidities h_1 and h_2 ($h_2 > h_1$), the boundary conditions induce a moisture gradient inside the specimen and hence moisture transport throughout the specimen (see Section 3.3.2). Under steady-state conditions, this specimen is theoretically "crossed" by a constant water vapour mass flux density J_v, from surface 2 to surface 1 (the other sides being sealed, see Fig. 5). In these conditions and in the case of small p_v gradient and small thickness e, the diffusion coefficient (and the "permeability") can be assumed to be constant within the range $[h_1; h_2]$ (and to correspond to $(h_1+h_2)/2$) and Eq. (7) reads (see Eq. (8)):

$$D_{ve} = \frac{RT}{M} \cdot \delta = \frac{RT}{M} \cdot \frac{J_v \cdot e}{p_{vs} \cdot (h_2 - h_l)} \tag{8}$$

Note that J_v is more exactly the mass flux density at the boundary (see Section 3.3.2), while the actual moisture flow inside the specimen involves both the liquid and vapour phases.

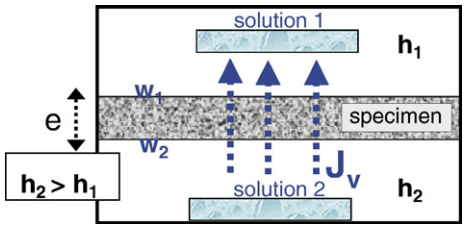

Fig. 5. Simplified scheme of the cup test set-up. w_1, w_2: water contents of the boundary layers. h_1, h_2: relative humidities in the compartments.

3.3.2. Cup test

According to the literature [11,20,21,22], the "permeability" to water vapour and the *effective* water vapour diffusion coefficient D_{ve} can be directly assessed, at the macroscopic scale under non-saturated and steady-state conditions (constant flux density), from the equations described in the previous section and by means of a cup test (see Fig. 5).

Such a test has been performed here. The experimental set-up is a cylindrical cell constituted of two compartments separated by the material specimen (3- to 6-mm thick slice) to be tested. In each compartment, the relative humidity is imposed by a different saturated salt solution (see Fig. 5, where $h_2 > h_1$). The temperature is constant and the total pressure is identical in the two compartments (p_{atm}). A silicon sealant is used to prevent moisture leakages between the cell walls and the specimen. After a transient period where the mass of the material specimen varies (according to its initial moisture state) [20,21], a linear water content gradient is theoretically established within the material specimen (steady-state regime). In these conditions, "diffusion" is assumed to take place between the two boundary layers (where $w_2 > w_1$) assumed to be permanently in equilibrium with the surrounding media, i.e. the compartments (the mass of the specimen does not vary anymore). As the device is provided by bottom and top openings, the mass of both salt solution 1 (linear increase within the steady-state regime, in the previously mentioned initial conditions) and salt solution 2 (linear decrease) can be monitored as a function of time. In addition, in this case both solutions can be controlled and renewed during the test (e.g. possible desaturation of solution 1). The precision of the balance used here is 0.001 g. The

steady-state range can hence be identified (after at least several months) and the flux density J_v "crossing" the specimen can be calculated (theoretically, J_v = outgoing flow J_{v1} = ingoing flow J_{v2} = constant [22]). The reiteration of the experiment for several couples (h_1, h_2) allows obtaining the evolution of the coefficients δ and D_{ve} *vs*. RH from Eq. (8).

3.3.3. Effective water vapour diffusion coefficient D_{ve} assessed from the cup test (under steady-state conditions) — experimental results and discussion

The D_{ve} values experimentally obtained by means of the cup test applied with various initial conditions, various couples (h_1, h_2) and Eq. (8) on concretes BO-SN and B30-A are plotted *vs*. average RH [$=(h_1+h_2)/2$] in Fig. 6a. Note that results on M25 can be found in [23] and "permeability" results obtained on CO and CH can be found in [21]. Fig. 6a shows that the variations of D_{ve} as a function of RH are not significant, except maybe within the very high and very low RH ranges. Moreover, the results obtained for the two concretes BO-SN and B30-A are very close. The values found here ($0.5–2.5 \cdot 10^{-7}$ m^2 s^{-1}) are in agreement with the data reported in the literature:

- D_{ve} = 5.01 and $10.05 \cdot 10^{-7}$ m^2 s^{-1}, for two different concretes in the case of a single cup test (0, 100%) applied to specimens previously dried at T = 110°C [24],
- $D_{ve} = 1–2 \cdot 10^{-7}$ m^2 s^{-1} measured by the "wet cup method" (50%, 93–100%) and $D_{ve} = 0.1–1 \cdot 10^{-7}$ m^2 s^{-1} by the "dry cup method" (0; 50%) for HPCs [25].

However, it can be mentioned that these three (standard) cup tests don't meet the requirement for a licit application of Eq. (8) (see Section 3.3.1).

Note that $D_{ve} \ll D_{v0}$, illustrating the hindering effects of the pore network (tortuosity, connectivity, constrictivity) and of its partial filling by the liquid phase for the vapour diffusion.

The D_{ve} values are plotted *vs.* average S_l in Fig. 6b and are compared to the results obtained by means of the formula $D_{ve}(S_l) = D_{v0} \cdot f(S_l, \Phi)$ and by using the analytical expression given by Millington for the resistance factor $f(S_l,\Phi)$ (see Eq. (9) [26]):

$$f(S_l, \Phi) = \Phi^{4/3} \cdot (1-S_l)^{10/3} \quad (9)$$

When S_l increases from 0 to 0.50, the experimental D_{ve} values seem to decrease in agreement with the analytical trend (since liquid "islands", as a result of the presence of a disconnected liquid phase, are regarded as an hindrance to vapour diffusion in this formula), but in a less marked manner. In particular, significantly lower experimental values are pointed out within the low S_l range. This illustrates that the proposed analytical formula is not appropriate. A calibration of the exponents could be needed or other effects of the pore system (connectivity, constrictivity) should be taken into account, since they can also influence the vapour transport. In addition, other mechanisms than "pure" Fickian diffusion can take place within this range. For example, Knudsen molecular diffusion [4] is known to reduce diffusion coefficients in narrow pores. More precisely, this transport mechanism is prominent when $r_p \ll \lambda/2$, where r_p is the pore radius and λ denotes the mean free path of water vapour molecules in the air ($\lambda \approx 100$ nm) [11]. Note that a comparison between, on the one hand coefficients calculated by means of Millington's formula, and on the other hand oxygen and CO_2 diffusion coefficients measured on mortars [27] and hydrogen diffusion coefficients measured on hcps [28], has also pointed out discrepancies (see [14,29]). The variations of D_{ve} when S_l increases from 0 to 0.50 can explain the trend observed for D_a (S_l) within this range (see Section 3.2.3 and Fig. 4).

When S_l increases from 0.50 to 1, the experimental trend seems consistent with the analytical one. However, few data are available here within the high S_l range. In addition, within the high S_l range values close to zero are provided by Millington's formula, whereas high experimental D_{ve} (or δ) values can be found, according to the literature [21,22,23,30], when the connectivity of the liquid phase is sufficiently high, depending

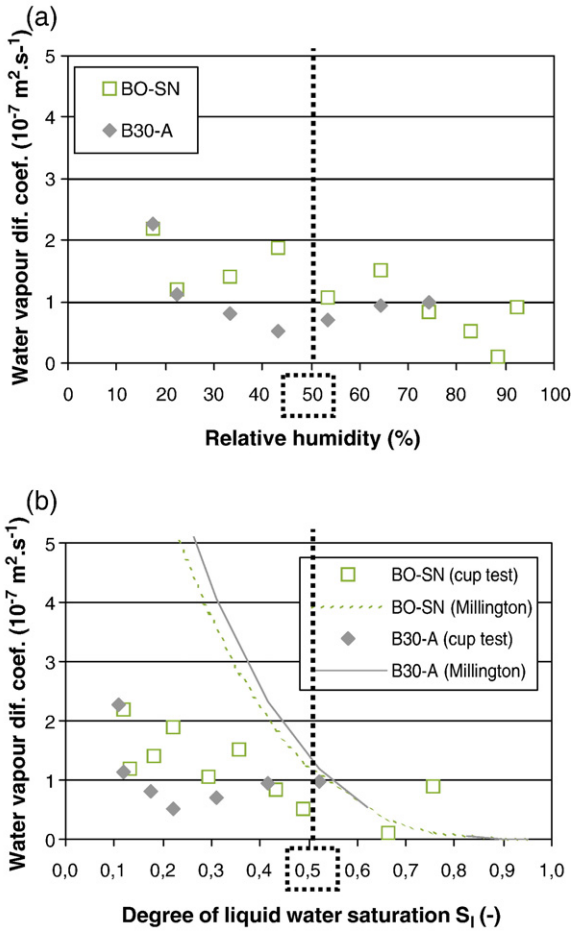

Fig. 6. *Effective* water vapour diffusion coefficient D_{ve} measured under steady-state conditions by means of the cup test, on concretes BO-SN (series 2*; W/C = 0.44) and B30-A (series 4; W/C = 0.50). Comparison with the analytical formula from Millington [26]. a) *vs.* average RH [$=(h_1+h_2)/2$]; b) *vs.* degree of liquid water saturation S_l.

on the hygral history and initial state of the test specimens. When the liquid phase is connected, the Darcian moisture transport under the liquid phase is prominent and in this case particularly high values of transport coefficients are expected (see Fig. 9).

All of this yields the conclusion that the cup test does not characterize the sole water vapour phase. Moreover, although D_{ve} is theoretically a "pure" transport property (as assessed under steady-state conditions), which should not include moisture–solid interactions, the experimental results appear to strongly depend on the hygral history and initial state of the test specimen, and D_{ve} does not exhibit a systematic trend of variation *vs.* S_l. As a matter of fact, hysteretical effects are pointed out in [21].

3.4. Component (D_v) associated with water vapour of the apparent moisture diffusion coefficient

3.4.1. Method of assessment from the cup test under steady-state conditions and from WVSI

If ones uses in the formula (displayed in Eq. (5)) of the component D_v of the *apparent* moisture diffusion coefficient, associated with the Fickian transport of water vapour according to the usual description of isothermal moisture transport, the expression of S_l given in Eq. (10):

$$S_l = \frac{w \cdot \rho_{app.dry}}{\Phi \cdot \rho_l} \tag{10}$$

where w denotes the mass water content and $\rho_{app.dry}$ the apparent bulk mass density of the dry material, along with Kelvin equation (see Eq. (11)), which can be used here, since p=constant=p_{atm}:

$$p_c = -\rho_l \cdot \frac{RT}{M} \cdot \ln h \tag{11}$$

the following Eq. (12) is obtained:

$$D_v = \frac{\delta}{\rho_{app.dry}} \cdot \frac{p_{vs}}{\left(\frac{dw}{dh}\right)} \tag{12}$$

Therefore, at the macroscopic scale and within the same experimental framework as described in Section 3.3.1, D_v can be computed from Eq. (13) (method 1):

$$D_v = \frac{\delta}{\rho_{app.dry}} \cdot \frac{p_{vs}}{\left(\frac{\Delta w}{\Delta h}\right)} \quad \text{(method 1)} \tag{13}$$

which requires the previous assessment of the "permeability" to water vapour δ (or D_{ve}) by means of the cup test under steady-state conditions and of the slope $\frac{\Delta w}{\Delta h}$ of the WVSI, desorption or adsorption isotherm depending on the experimental conditions of the cup test, within the range $[h_1; h_2]$.

The calculation can also be performed from Eq. (14) (method 2):

$$D_v = \frac{J_v}{\rho_{app.dry}} \cdot \frac{e}{w_2 - w_1} \quad \text{(method 2)} \tag{14}$$

by measuring the flux crossing the sample surface during the cup test in steady-state conditions and by deducing the water contents w_1 and w_2 of the boundary layers from the experimental WVSI of the tested material.

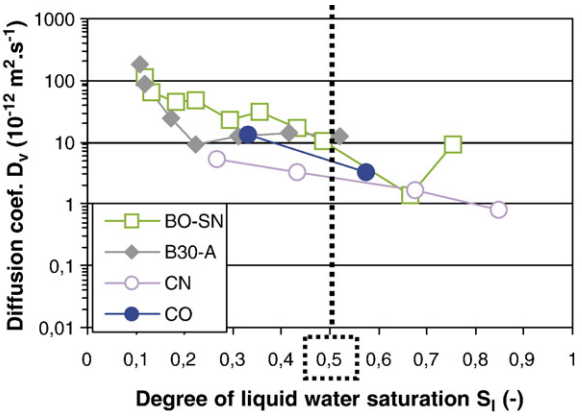

Fig. 7. Diffusion coefficient D_v *vs.* degree of liquid water saturation S_l, assessed under steady-state conditions by means of the cup test, on hcps CN and CO and on concretes BO-SN and B30-A, and by using the respective water vapour desorption isotherms.

3.4.2. Experimental results and discussion

It has been checked that methods 1 and 2 provided the same results as regards the assessment of D_v. The experimental coefficients D_v obtained on concretes BO-SN and B30-A are plotted *vs.* S_l in Fig. 7. Here, the water vapour desorption isotherms (WVDIs) of the materials have been used. The results provided in [2] on hcps CO and CN are also reported in the figure. Whatever the material tested, the results exhibit similar trends and order of magnitude over the whole S_l range. In particular, very similar D_v are obtained within the low S_l range. Most values lie within the range: $10^{-12} \leq D_v(S_l) \leq 10^{-10}$ m² s⁻¹.

The experimental results show that $D_v > D_a$ (see Figs. 4 and 7). Such a trend is consistent with the results published in the literature [4,6], but inconsistent with Eq. (4). In order to explain this finding, Philip and de Vries [17] explained that the liquid–vapour interactions (see Section 3.3) are not taken into account in the theory (e.g. evaporation–condensation through liquid "islands" enhances the transport, according to Daian [4]), and Daian [4] suggested that Eq. (13) yields an overestimation of the actual water vapour diffusion coefficient in the material. Likewise, if, according to the conclusion of Section 3.3.3, the mass flux density J_v measured by the cup test is likely to result from both liquid water movements and water vapour diffusion, therefore the experimental D_v value will be overestimated compared to the theoretical one. Moreover, this observation questions the relevance of the usual treatment of the cup test.

4. Liquid water permeability — definition, methods of assessment and results

4.1. Definition

Among the transport properties, the liquid water permeability $K_l k_{rl}(S_l)$ (see Section 3.2.3) of a non-saturated medium governs the (advective) transport of liquid water according to the extended Darcy's law. This law characterizes the viscous flow of an incompressible and non-reactive fluid under a total

pressure gradient and reads in a one-dimensional scheme along a Ox-axis (Eq. (15)):

$$v_l = -\frac{K_l}{\eta_l} \cdot k_{rl}(S_l) \cdot \frac{\partial p_l}{\partial x} \quad (15)$$

where v_l denotes the filtration velocity of liquid water and p_l the liquid pressure.

The permeability $K_l k_{rl}(S_l)$ thus depends on the characteristics of the fluid, on the pore network (pore sizes, connectivity, …) and other voids (microcracks, paste-aggregate interfacial zone, …) of the material, as well as on the hygral state of the test specimen.

4.2. Assessment of "intrinsic" liquid water permeability K_l — methods available

The "intrinsic" liquid water permeability K_l (permeability at $S_l = 1$) can easily be assessed by direct measurement for highly permeable cementitious materials. The method can be summarized as follows: vacuum saturation in water, application of a liquid pressure (in laminar flow conditions) on one side of the specimen, measurement of the flow on the other side, and calculation of the permeability from Eq. (15) when the steady-state regime is reached.

For some kinds of materials, this parameter can also be estimated by the Katz–Thompson relationship, originally developed for sedimentary rocks and based upon the percolation theory [31,32], when the critical (i.e. breakthrough) pore diameter and the formation factor F of the material are known [33,34,35,36,37,38]. The so-called formation factor of the porous medium can be calculated as the ratio of electrical conductivities or of diffusion coefficients (in the porous medium and in bulk liquid). However, this relationship has rather been validated for normal-strength materials, and more particularly for hardened cement pastes.

Conversely, it is widely recognized that the direct measurement (by conventional devices) of liquid water permeability is difficult in the case of weakly permeable materials [38,39,40].

Furthermore, the correlation between liquid water permeability and gas permeability is not trivial for cement-based materials and is very dependent on the mix-composition (see Section 5.4). Therefore, it is difficult to deduce the liquid water permeability of weakly permeable materials from gas permeability measurement, even if the latter is easier.

Hence, in the case of weakly permeable materials, advanced experimental devices (see for example [41,42]) or indirect methods are required, in order to assess this basic property. As regards indirect methods, important work on this topic has been reported by Scherer (e.g. rapid methods such as beam bending or thermopermeametry, first applied to gels and later extended to more rigid materials and recently to cement pastes [43,44,45,46]).

4.3. Assessment of "intrinsic" liquid water permeability K_l by indirect method based upon numerical inverse analysis from a drying experiment

4.3.1. Description of the method

An indirect method (based upon inverse analysis), which combines experiments and numerical model, can be used to assess liquid water permeability when no relevant direct method is available or applicable. This method, proposed by Coussy et al. [47], is based upon the analysis of the relative mass loss *vs.* time plot (kinetics), associated with a drying test at a given RH and at constant T (see the description of this test in [1]), by means of an isothermal moisture transport model, and upon the determination of a few basic material properties (the porosity Φ and the WVDI are required as inputs of the model, see Section 4.3.2). According to Section 4.2, such a method is particularly useful for weakly permeable materials. When the model and the mentioned input data are available, this method has in particular the advantage to be based on a single simple experiment, which does not require any specific apparatus and which can be carried out easily in every laboratory.

Thanks to the conclusions provided by the modelling and the analysis of isothermal drying of cementitious materials performed by Mainguy in [16], a simplified modelling has been proposed in [47,48]. This model considers solely the transport of liquid water according to Darcy's law, with no vapour diffusion, and assumes $p_c = p_{atm} - p_l$ and no evaporation within the finite-size material sample. This yields a single non-linear diffusion-type equation, which includes only the parameters associated with liquid water (i.e. $D_l(S_l)$, see Eq. (5)). Such a simplified model can be implemented for assessing the "intrinsic" liquid water permeability: K_l is deduced from the best fitting of the predicted relative moisture losses on the values observed for the sample submitted to the drying experiment (see Fig. 8 and the description of the corresponding experiments and computations in [48,49]). The calculation can be carried out whatever the initial state of the sample: vacuum-saturated, water-cured (see Fig. 8b) or self-desiccated (see Fig. 8a), provided that the gradient between the initial and boundary RHs is large enough to keep an appropriate accuracy.

This method has been applied here, in order to assess the "intrinsic" liquid water permeability K_l of various materials.

4.3.2. Required parameters

In addition to initial and boundary conditions, a basic input required by the model is the derivative of the capillary pressure curve $p_c(S_l)$ of the material (see the expression of $D_l(S_l)$ in Eq. (5)). The capillary pressure curve has to be derived from the experimental WVDI by using Kelvin equation (along with the bulk porosity Φ and the apparent bulk mass density of the dry material $\rho_{app.dry}$, see Eqs. (10) and (11)) [48,50]. Moreover, a continuous curve is required, in order to facilitate the inclusion into the model. Among the various formulas (such as parametric equations) proposed in the literature, a good fitting on the experimental capillary pressure curves can be obtained through the analytical formula proposed by van Genuchten [51] (see Eq. (16)):

$$p_c(S_l) = a \cdot (S_l^{-1/m} - 1)^{1-m} \quad (16)$$

where a and m are fitting parameters, which depend on the microstructure (in particular on the connectivity of the pore system) of the material.

Other types of fitting are possible (polynomial, …). The slope of the capillary pressure curve can also be assessed in a simpler

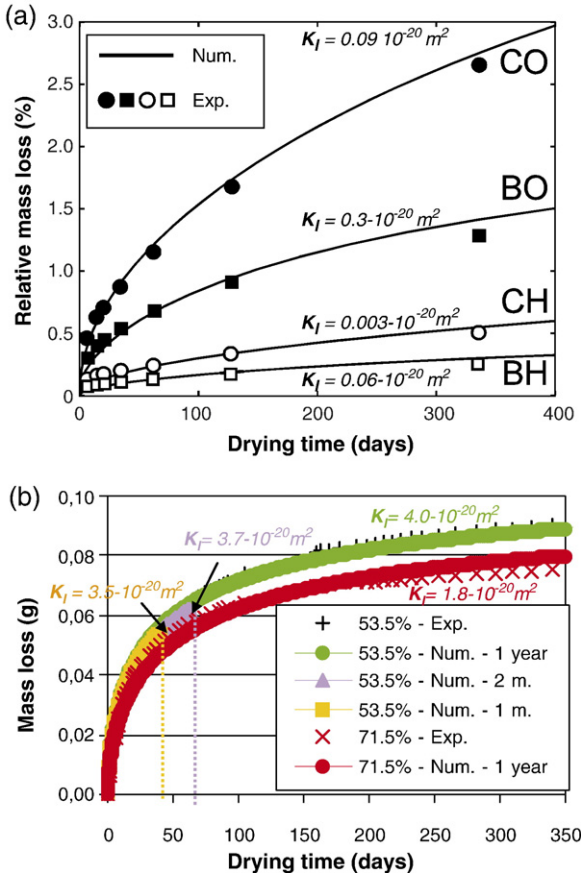

Fig. 8. Illustration of the principle of the indirect method for assessing "intrinsic" liquid water permeability K_l and numerical results. a) Fitting on experimental relative mass losses (drying time = 1 year), for Ø160 × 100-mm samples of CO, CH, BO and BH submitted to RH = 50% at T = 21 ± 1 °C, after 2-year sealed curing [48]. b) Fitting on experimental relative mass losses, in the cases of drying time = 1 year, 2 months and 1 month, for Ø110 × 100-mm samples of concrete M25 submitted to RH = 53.5% and 71.5% at T = 21 ± 1 °C, after 1-year water curing [49].

way from three experimental plots within the considered RH range. However, fitting according to Eq. (16) gives the advantage of allowing also prediction of the relative permeability to liquid water $k_{rl}(S_l)$ (see Section 4.4), which is required for the implementation of the model, and to gas (see Section 5.3), from parameter m and from analytical formulas. The fact that experimental WVDIs provide S_l (= $S_l$max) < 1 at RH = 100% with the tested materials [1], whereas Eq. (16) provides $S_l$max = 1, can be taken into account in the analytical formula by using S_l/S_lmax instead of S_l (see for example [52]).

4.4. Assessment of relative permeability to liquid water $k_{rl}(S_l)$ from WVSI and analytical formula

Few experimental data are available as regards the relative permeability of cement-based materials to gas (see Section 5.3) and even less to liquid water. Nevertheless, analytical formulas are proposed in the literature. For example, Eq. (17), where appears the parameter m derived from the analytical expression of the capillary pressure curve (see Eq. (16)), has been proposed by van Genuchten in [51] by using Mualem's model [53]:

$$k_{rl}(S_l) = \sqrt{S_l}\left(1-\left(1-S_l^{1/m}\right)^m\right)^2 \quad (17)$$

In addition, Savage and Jenssen have shown that this formula, originally developed in the soil sciences, could be applied to cement-based materials [54].

The relative permeability to liquid water $k_{rl}(S_l)$ has been assessed here by using this formula.

4.5. Numerical, analytical and experimental results

4.5.1. Relative permeability to liquid water $k_{rl}(S_l)$

The results obtained by using Eq. (17) with the values m = 0.4854, 0.4396 and 0.4191 deduced from Eq. (16) and from the experimental WVDIs for concretes BH, BO and M25 respectively, are displayed in Fig. 9. A drastic influence of S_l is observed. In particular, the curve provides $k_{rl} \approx 0$ for $S_l \leq 0.40$ (i.e. RH ≤ 50%, for BO). This can be explained by the fact that, within this range, the liquid phase is disconnected (liquid "islands") and no significant (Darcian) transport under liquid form can therefore occur. On the other hand, within the high S_l range, k_{rl} greatly increases with S_l. This explains the variations of $D_a(S_l)$ observed within this range where liquid transport is prominent (see Fig. 4 in Section 3.2.3). Furthermore, slight differences are observed between the various materials (see also the results obtained for CO and CH and displayed in [49,50]). In particular, the curves obtained for BO and M25 are nearly the same. This confirms the negligible influence of the material pore structure characteristics (in particular the WVDI) on k_{rl}.

4.5.2. "Intrinsic" liquid water permeability K_l obtained by numerical inverse analysis

The K_l results obtained by numerical inverse analysis for a set of hcps and concretes are presented in Table 5 and in Fig. 8. Fig. 8 illustrates that the method is applicable not only for weakly permeable materials (e.g. CH and BH) [48], but also for highly permeable concretes such as M25 [49].

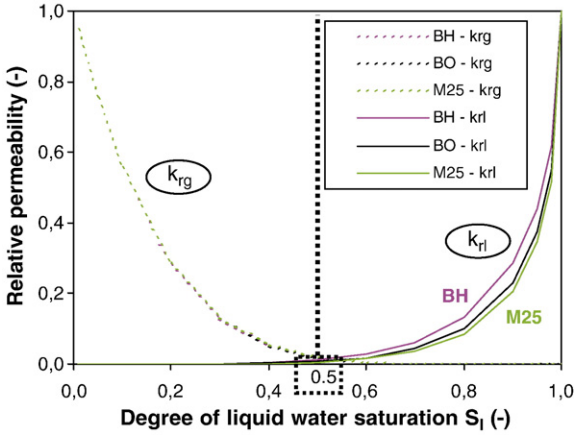

Fig. 9. Relative permeabilities to liquid water (k_{rl}) according to the analytical formula given in [51] and to gas (k_{rg}) according to the analytical formula given in [30] *vs.* degree of liquid water saturation S_l, for concretes BH, BO and M25.

Table 5
Comparison between the "intrinsic" permeabilities obtained by various methods for several materials (3–6-month old, before preconditioning and testing)

Material	Concrete	Concrete	hcp	Concrete	hcp
	M25	BO	CO	BH	CH
Inverse of the formation factor 1/F (−)	$3 \cdot 10^{-3}$	$0.9 \cdot 10^{-3}$	$1.7 \cdot 10^{-3}$	$3.7 \cdot 10^{-5}$	$2.3 \cdot 10^{-7}$
"Intrinsic" gas permeability K_{ig} (m^2) (S_l=0)	$3 \cdot 10^{-16}$	$54 \cdot 10^{-18}$	$130 \cdot 10^{-18}$	$25 \cdot 10^{-18}$	$<10^{-19}$
"Intrinsic" liquid water permeability K_l (10^{-20} m^2) (S_l=1) [direct measurement]	9900	8.8			
"Intrinsic" liquid water permeability K_l (10^{-20} m^2) (S_l=1) [Katz–Thompson formula]	3.6	0.8	0.7	0.006	$<10^{-4}$
"Intrinsic" liquid water permeability K_l (10^{-20} m^2) (S_l=1) [inverse analysis] [14,49,55]	4.2 (0)–1.6 (4)				
	4.0 (1)–1.8 (5)	0.30 (1)	0.09 (1)	0.06 (1)	0.003 (1)
	3.7 (2)	0.36 (2)	0.08 (2)	0.08 (2)	0.004 (2)
	3.5 (3)	0.38 (3)	0.07 (3)	0.002 (3)	0.001 (3)

(0): RH=53.5%, drying time=2.5 years.
(1): RH=50 or 53.5%, drying time=1 year.
(2): RH=50 or 53.5%, drying time=2 months.
(3): RH=50 or 53.5%, drying time=1 month.
(4): RH=71.5%, drying time=2.5 years.
(5): RH=71.5%, drying time=1 year.

In Table 5 are reported the K_l values obtained by performing numerical inverse analysis after various drying times for every tested material (and at two different RHs, in the case of M25) [14,49,55]. The corresponding drying kinetics (relative mass loss *vs*. drying time plots) are displayed for concrete M25 in Fig. 8b. Fig. 8b and Table 5 point out that the monitoring of the drying kinetics during only one month for normal-strength materials is sufficient to obtain an acceptable accuracy for K_l. As far as HP materials are concerned, at least two months are required; for shorter periods, the numerical curve in the long term is far from the experimental plots and the K_l results are far from the average value (see in Table 5 the crossed out values obtained after 1-month drying with BH and CH). However, it is worth reminding (see Section 4.2) that quicker (but more sophisticated) methods can be used, in order to assess K_l within a few minutes to a few hours (see [44,46] or [56,57]).

Moreover, the RH range associated with the drying experiment seems to have only a slight influence on the permeability value (see Fig. 8b and Table 5).

Note furthermore that same values of permeability were found in [49] with either the complete [16] or the simplified model proposed in [47,48], confirming thereby the relevance and the validity of the simplified model.

4.5.3. "Intrinsic" liquid water permeability K_l — comparison between various methods

The K_l values provided by various methods are compared in Table 5: direct measurement with conventional device (for permeable materials) as described in Section 4.2, calculation according to the Katz–Thompson formula, and numerical inverse analysis from a drying experiment. The formation factor F involved in the Katz–Thompson formula is calculated here (see Table 5) as the ratio of (effective) chloride diffusion coefficients (with the chloride diffusion coefficient in bulk water $D_{0(Cl^-)}=1.484 \cdot 10^{-9}$ m^2 s^{-1}), while the critical pore diameter is obtained from MIP measurement.

Whatever the method, the permeabilities obtained on HP materials are significantly lower than those recorded on normal materials (see Table 5).

A good agreement is observed between the permeability estimated by the Katz–Thompson relationship and the one predicted by inverse analysis for M25 and BO. The values are also in agreement with those reported in the literature. In addition, the same ranking is obtained for the various materials tested. Therefore, these methods appear as equivalent alternative ways for assessing the liquid water permeability of normal-strength materials. On the other hand, a significant discrepancy is observed between these two methods for the weakly permeable materials. This questions the validity of the Katz–Thompson formula in this case (as already discussed in the literature [33,34,35,36]) and explains that some adaptations of the formula have already been proposed. Furthermore, this may indicate that, in the case of weakly permeable materials (in particular HPCs), inverse analysis is the sole possible method among the two discussed methods.

A very large difference is highlighted between, on the one hand the value obtained here by direct measurement and the values reported in other publications, and on the other hand the permeability estimated by inverse analysis (or by the Katz–Thompson formula), for the highly permeable concrete M25. A lot of phenomena are likely to contribute to the large difference observed. As regards the direct measurement, all the defects and big voids present in such a low-grade concrete (W/C=0.84) will contribute to increase the liquid flow (as they constitute preferential paths for the flow) and therefore the permeability. As these defects and big voids will not influence in a so great extent in the long term the drying kinetics used in the numerical inverse method, significant differences will be recorded in the results. As regards the Katz–Thompson formula, diffusion coefficients have been used here, which are neither drastically influenced by defects and big voids (the diffusion kinetics is determined by the transport in the smallest pores). In addition, the critical diameter used in the formula has been assessed here by ignoring the (pore volume) mode linked to the biggest pores. It can be added as regards the numerical inverse method that the use for the highly permeable concrete M25 of a simplified modelling, which considers the sole transport of liquid water according to Darcy's law (without water vapour diffusion and

without evaporation within the sample, see Section 4.3.1) can be questionable. As a matter of fact, it has been highlighted in [14], by using a refined modelling (improved formulas for relative gas permeability and for *effective* water vapour diffusion coefficient, …), that the transport in the gas phase was not negligible in such a material. It can be seen in Table 5 that a better agreement is observed between the permeability obtained by direct measurement and the one estimated by numerical inverse analysis (or by the Katz–Thompson formula) for the normal-strength concrete BO. The difference (i.e. factor of 25) recorded with this material can be attributed at least partially to the fact that the permeameter worked in the case of this good-quality concrete at the limit of admissible pressures. Consequently, some uncertainty can be expected in the recorded permeability. It can be added that the K_l values obtained by inverse analysis on CO, CH, BO and BH seem correct, or at least appropriate for the quantification and the prediction of moisture transport, since they yielded numerical moisture profiles consistent with experimental ones in the case of a drying process in well-defined conditions [48]. In addition, the same order of magnitude has been found in the literature by means of numerical models [56] or experimentally on mortars [58]. Therefore, it can be considered that the indirect method based upon inverse analysis is validated for such materials. Nevertheless, one has to keep in mind that the results depend on the analytical formula selected for the WVDI (and for the relative permeability).

5. Assessment of gas permeability and comparison with liquid water permeability

5.1. Apparent gas permeability — definition and direct measurement

By assuming laminar flow under steady-state conditions, the *apparent* gas permeability of a dry material ($S_l=0$), denoted K_{ag} (in m^2), can be calculated from direct measurement (one side of the test specimen is submitted to a constant inlet gas pressure p), by using Eq. (18) derived from Hagen–Poiseuille's law when applied to compressible fluids (gases) [59]:

$$K_{ag} = \frac{2 \cdot Q \cdot p_{atm} \cdot e \cdot \eta_g}{A \cdot (p^2 - p_{atm}^2)} \tag{18}$$

where Q is the outgoing volume gas flow (in $m^3\ s^{-1}$) measured at the opposite side of the test specimen under steady-state conditions, while A and e are respectively the cross-sectional area and the thickness (in the flow direction) of the test specimen, and η_g denotes the dynamic viscosity of the gas.

This *apparent* gas permeability K_{ag} can be assessed by means of the Cembureau constant head gas permeameter [59], according to the AFPC-AFREM test procedure described in [60], and by using oxygen. Before testing, the ∅150 × 50-mm samples are water-cured and then dried according to [60]: ventilated oven drying at $T=80\pm5$ °C for 28 days, followed by ventilated oven drying at $T=105\pm5$ °C until the observed relative mass loss is less than 0.05% between two consecutive readings at a time interval of 24 hours. At the end of the process, the test specimen is assumed as "dry" ($S_l=0$).

K_{ag} is not only dependent on the pore structure of the material, but also varies with the applied mean pressure $p_m=(p+p_{atm})/2$.

5.2. "Intrinsic" gas permeability — Klinkenberg's concept

It is possible to assess the "intrinsic" gas permeability of a dry material K_{ig} (in m^2), which is solely a characteristic of the void network (it is independent of the applied mean pressure and theoretically of the fluid, liquid or gas), and which is associated with pure viscous transport, by using Klinkenberg's method [61] based on Eq. (19):

$$K_{ag} = K_{ig} \cdot \left(1 + \frac{\beta}{p_m}\right) \tag{19}$$

where the so-called Klinkenberg's constant β is a characteristic of both the porous medium and the percolating fluid.

Note that here "intrinsic" has not the same meaning as in the case of liquid water permeability.

This method has already been used by various authors [62,63,64] and has been applied in [65] to same concretes as BO-SN, BO and BH. According to Eq. (19), it consists in performing permeability tests and measuring K_{ag} at different inlet pressures, and then plotting the data *vs.* $1/p_m$. K_{ig} is the limit value of K_{ag} when $1/p_m$ tends towards 0 (i.e. when p_m tends towards infinity). K_{ig} is thus deduced by extrapolation from the intercept with the Oy-axis through a linear fitting. βK_{ig} is the slope of the straight line.

The Klinkenberg's concept [61] is based on the observation that the measured gas flow is higher than the value theoretically expected, as a result of slip effects in addition to pure viscous flow. The author explains by this concept the fact that, for a given material, gas permeability is higher than liquid water permeability, and can be equal solely in the case of highly permeable materials (see Section 5.4).

5.3. Relative permeability to gas $k_{rg}(S_l)$ — assessment from WVSI and analytical formula

The "intrinsic" gas permeability at a given degree of gas saturation S_g reads $K_{ig}k_{rg}(S_g)$, where $k_{rg}(S_g)$ is the relative permeability to gas ($k_{rg} \le 1$) and $S_g=1-S_l$. In order to better illustrate the fact that k_{rg} quantifies the reduction of the gas permeability induced by the presence of the liquid water phase in the pore system, and in order to study experimentally and analytically the variations of k_{rg} as a function of the degree of liquid water saturation S_l (as for k_{rl}), k_{rg} will be expressed as a function of the variable S_l. As in the case of the relative permeability to liquid water, k_{rg} can be derived from WVSIs, thanks to analytical formulas proposed in the literature (see e.g. Eq. (20)):

$$k_{rg}(S_l) = (1-S_l)^{\xi} \cdot \left(1-S_l^{1/m}\right)^{2m} \tag{20}$$

where m is the same parameter as in k_{rl} formula and ξ is another fitting parameter.

Note that the Klinkenberg's constant β is also dependent on S_l: when S_l decreases, β increases [14,64,65].

Eq. (20) has been applied here to concretes BO and BH with the values given in Section 4.5.1 for parameter m and with:

- $\xi = 0.5$ according to Parker et al. [67] (and applied in [16,48,50]). Parker et al. found this expression when extending Mualem's model [53] to the non-wetting phase, in the case of soils,
- $\xi = 5.5$ according to Monlouis–Bonnaire [30] for cementitious materials.

Note in addition that $\xi = 1/3$ was proposed by Luckner et al. in [68].

The analytical results obtained for the relative permeability to gas $k_{rg}(S_l)$, by applying Eq. (20), are compared to experimental data in Fig. 10a and b, for BO and BH respectively. The experimental data were obtained by applying Klinkenberg's method at various S_l, in order to assess the "intrinsic" gas permeability at a given S_l. These various S_l were obtained by using two drying procedures (see [65]): on the one hand, step-by-step drying at $T = 45$ °C and at various RHs by means of saturated salt solutions, and on the other hand, oven drying according to [60] (see Section 5.1). A drastic influence of S_l is observed, as already reported in the literature (e.g. [66]), and a far better agreement with experimental data is highlighted in the case of the analytical formula proposed in [30], in spite of some differences within the mid S_l range. The application of the formula proposed in [67] to the hcps CO and CH (see [48,50]) shows quite similar curves to that obtained for concretes BO and BH. Therefore, this latter formula, originally developed for soils, does not seem relevant for normal-strength and HP cementitious materials.

In Fig. 10a and b is also displayed the fitting on the experimental data by using a ln function, according to [64,65]. The results show that experimental data can correctly be approximated by using ln functions, although such a fitting has no predicting feature.

The results obtained by applying Eq. (20) to BH, BO and M25 are compared in Fig. 9. Similarly as for k_{rl}, the identical curves obtained point out that the material characteristics have no influence on k_{rg}. This finding is confirmed by the experimental results obtained on BO and BH and by fitting according to ln functions (see Fig. 10c). Such a "universal" relationship $k_{rg} = k_{rg}(S_l)$ can therefore be assessed from a single material and can be used (and included as input data in models) for every other one.

5.4. Comparison between gas and liquid water permeabilities

The experimental "intrinsic" gas permeabilities (i.e. when p_m tends towards infinity) obtained in the case where $S_l = 0$ (i.e. for dry samples) can be compared to the measured and calculated intrinsic liquid water permeabilities (i.e. at $S_l = 1$) for various hcps and concretes (see Table 5). Theoretically, if the fluids were neutral with respect to the material, these two parameters should be equal. This has also been pointed out experimentally. For example, Gross and Scherer [69] found a good accordance between intrinsic (CO_2) gas and (ethanol) liquid permeabilities

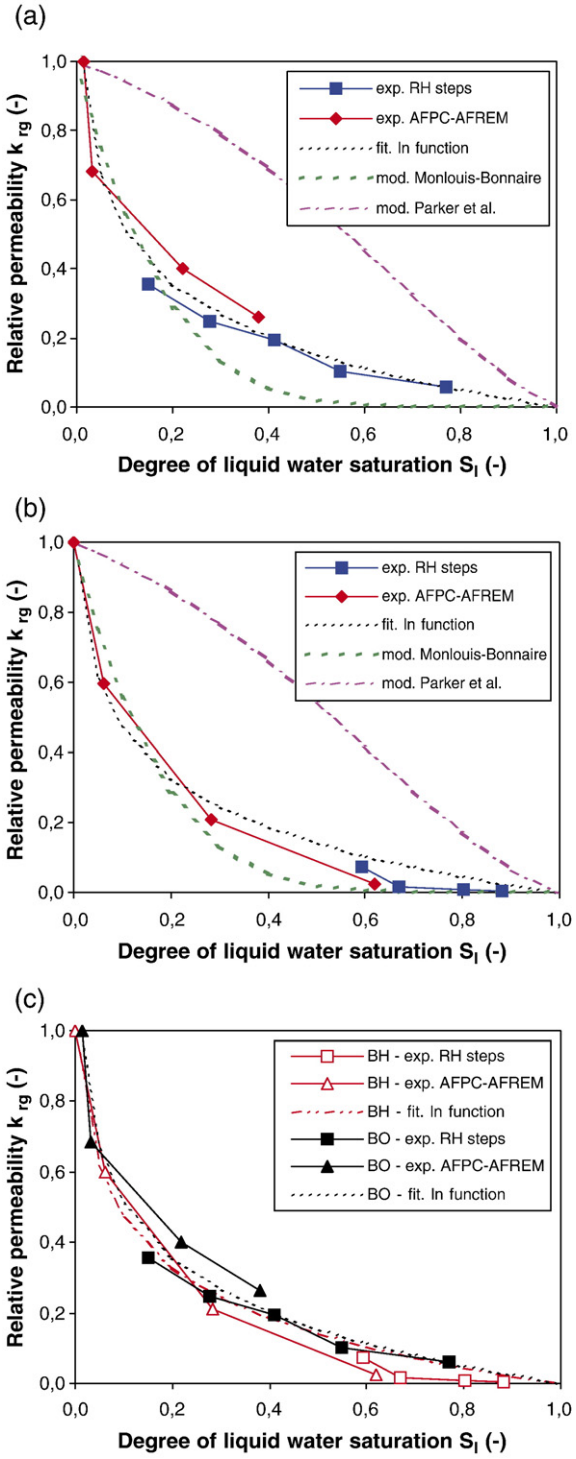

Fig. 10. Relative permeability to gas (k_{rg}) *vs.* degree of liquid water saturation S_l, assessed by various methods (direct measurement and analytical formulas). a) Concrete BO; b) concrete BH; c) concretes BO and BH.

of highly porous silica aerogel measured respectively by dynamic pressurization and beam bending [43,44]. Likewise, a difference of 40±10% has been reported in [57] between argon and ethanol permeabilities measured by pulse test on normal mortar (see also [40,56]).

Here, a difference of several orders of magnitude is observed between gas and liquid water permeabilities for the good-quality

materials CO, CH, BO and BH (gas permeability > liquid water permeability). Such differences have already been reported in the literature [38,39,61,62]. For example, Loosevelt et al. in [56] found similar values for argon and ethanol permeabilities with mortars, but the liquid water permeability was systematically lower. The difference observed here was expected, given the various physicochemical processes that may occur during the tests carried out: cracking during the drying process prior to gas permeability measurement, water–solid interactions during the drying test used for the indirect method (K_l is determined within the transient regime), water–solid interactions and other phenomena during the course of liquid water permeability testing (ongoing hydration [70], crack-healing [70,71], self-sealing [70,72], or leaching) in particular if the test takes a long time, …. Therefore, for weakly permeable materials, when the liquid water permeability cannot be measured, it cannot either be deduced from gas permeability measurement. As expected (see Section 5.2), a better agreement (one order of magnitude difference) is obtained between the liquid and gas permeabilities measured on the low-grade concrete M25.

6. Concluding remarks

Various results and experimental/analytical/numerical tools are presented in this paper. A database useful for further researches is thus available, in particular for the analysis and the physically-based modelling of transport/degradation processes and associated deformations.

Water vapour desorption–adsorption experiments are revealed as essential tools for durability evaluation and prediction. These experiments not only provide moisture properties and microstructure characteristics [1], but also transport properties. For example, by adding to water vapour sorption experiments a drying test at a given RH (and by using a moisture transport model), or a cup test, or a gas permeability test on a dry sample, it is possible to assess respectively liquid water permeability, diffusion coefficient associated to Fickian transport of water vapour, or gas permeability *vs*. the degree of saturation. Moreover, the *apparent* moisture diffusion coefficient *vs*. the degree of saturation can be directly deduced through the analysis of sorption kinetics.

In this paper, the drastic influence of the degree of liquid water saturation has been quantified on the experimental diffusion coefficients, as well as on the liquid water and gas permeabilities. In addition, it is found that diffusion coefficients are dramatically dependent on moisture history and test conditions [6,8,10]. The results presented in this paper show that, owing to the complex phenomena that take place during drying–wetting processes (in particular water–solid interactions and occurrence of combined vapour and liquid transport) and the mentioned moisture history dependency, inadequacy can arise between the diffusion coefficients involved in the theoretical description and those actually measured. It is therefore difficult to identify a "universal" durability indicator [40], which has to meet both the theoretical relevance and a reliable assessment by a well-defined procedure, among these diffusion coefficients, and to select the appropriate coefficient for inclusion as input data in models. Likewise, the "intrinsic" permeability of the materials tested in this study is obviously dependent on the fluid (liquid water or oxygen gas), probably as a result of the various phenomena that take place during the experiments (in particular, water–solid interactions). This finding, in addition to the results obtained here by various methods as regards liquid water permeability and to the results reported in the literature, points out the difficulty to assess actual intrinsic transport properties for cementitious materials. In particular, the concept of intrinsic permeability independent of the permeating fluid does not seem relevant for cementitious materials when liquid water is regarded, except maybe for highly permeable materials. But liquid water permeability is even so required for the quantification and the prediction of moisture and moisture-coupled transport processes. This implies in particular that two distinct gas and liquid water permeabilities have to be included as input data in models, as illustrated in [14].

It can be concluded that transport property results require reference to the moisture history, preconditioning, test methods and calculation formula used. These data are indispensable for a correct understanding (e.g. in order to deduce in which governing equation the coefficient is involved), interpretation and use of these results. Moreover, the origin of the discrepancies recorded between various methods still remains to be thoroughly clarified. This will help to improve the test procedures, and to make them appropriate to the whole range of concrete mixtures (from low-grade to ultra-high-performance concretes), since transport properties are of major practical interest.

Acknowledgments

The author is grateful to J. Godin and M. Pithon (LRPC Angers), for their contribution in the "cup tests", as well as to P. Belin and J. Gawsewitch (LCPC Paris), who contributed to the assessment of the moisture diffusion coefficient. The author gratefully acknowledges O. Coussy (LMSGC Marne-la-Vallée), M. Mainguy and M. Thiery (LCPC), who performed moisture transport modelling and numerical simulations. The author is also indebted to M. Thiery for helpful discussions on moisture transport and to G. Villain (LCPC) for her collaboration in the experimental work on gas permeability. The tritiated water diffusion tests were carried out at CEA Saclay by P. Lovera.

References

[1] V. Baroghel-Bouny, Water vapour sorption experiments on hardened cementitious materials. Part I: Essential tool for analysis of hygral behaviour and its relation to pore structure, Cem. Concr. Res. accepted for publication.

[2] V. Baroghel-Bouny, G. Bastian, J. Godin, A. Khelidj, P. Lovera, H. van Damme, Diffusion and moisture diffusivity in hardened cement pastes and concretes: comparative study of the test methods (in French), in: V. Baroghel-Bouny (Ed.), Proc. of Scientific Seminar "Transferts 2000", April 6–7, 2000, Paris, France, 2000, pp. 163–170.

[3] Z.P. Bazant, L.N. Najjar, Nonlinear water diffusion in nonsaturated concrete, Mater. Constr. 5 (25) (1972) 3–20.

[4] J.F. Daian, Condensation and isothermal water transfer in cement mortar — part I: pore size distribution, equilibrium water condensation and imbibition, Transp. Porous Media 3 (1988) 563–589.

[5] D. Xin, D.G. Zollinger, G.D. Allen, An approach to determine diffusivity in hardening concrete based on measured humidity profiles, Adv. Cem. Based Mater. 2 (1995) 138–144.
[6] O.C.G. Adan, Determination of moisture diffusivities in gypsum renders, Heron 40 (3) (1995) 201–215.
[7] B. Perrin, S. Bonnet, Experimental results concerning combined transport of humidity and chloride in non steady state, in: L.O. Nilsson, J.P. Ollivier (Eds.), Proc. of 1st Int. RILEM Workshop "Chloride penetration into concrete", Oct. 15–18, 1995, Saint-Rémy-lès-Chevreuse, France, RILEM, Paris, 1997, pp. 302–314.
[8] B. Perrin, V. Baroghel-Bouny, L. Chemloul, Methods of determination of the hydric diffusivity of hardened cement pastes (in French), Mater. Struct. 31 (208) (1998) 235–241.
[9] C. Leech, D. Lockington, P. Dux, Unsaturated diffusivity functions for concrete derived from NMR images, Mater. Struct. 36 (260) (2003) 413–418.
[10] A.A.J. Ketelaars, L. Pel, W.J. Coumans, P.J.A.M. Kerkhof, Drying kinetics: a comparison of diffusion coefficients from moisture concentration profiles and drying curves, Chem. Eng. Sci. 50 (7) (1995) 1187–1191.
[11] V. Baroghel-Bouny, Characterization of cement pastes and concretes — methods, analysis, interpretations (in French), Ph.D. Dissertation ENPC (LCPC Publ., Paris, 1994), 468 pp.
[12] J. Crank, The Mathematics of Diffusion, 2nd Ed.Oxford Science Publications, UK, 1975.
[13] C. Hall, W.D. Hoff, Water Transport in Brick, Stone and Concrete, Spon Press, London, 2002.
[14] M. Thiery, V. Baroghel-Bouny, N. Bourneton, G. Villain, C. Stefani, New approach of moisture transport modelling in concrete in (French), to Revue Européenne de Génie Civil, in press.
[15] A. Delagrave, J. Marchand, M. Pigeon, Influence of microstructure on the tritiated water diffusivity of mortars, Adv. Cem. Based Mater. 7 (1998) 60–65.
[16] M. Mainguy, Non-linear diffusion models in porous media. Application to leaching and to drying of cementitious materials (in French), Ph.D. Dissertation ENPC, Paris, Sept. 1999, 255 pp.
[17] J.R. Philip, D.A. de Vries, Moisture movement in porous materials under temperature gradients, Transactions, Am. Geophys. Union 38 (2) (1957) 222–232.
[18] J.R. Philip, Physics of water movement in porous solids, Spec. Rep. n° 40, Highway Research Board, Washington, D.C., 1958, pp. 147–163.
[19] O. Coussy, Mechanics of Porous Continua, John Wiley and Sons, 1995.
[20] P. Delcelier, Vapour transfers (in French), Cah. CSTB 298 (2322) (1989) 1–18.
[21] V. Baroghel-Bouny, B. Perrin, L. Chemloul, Experimental determination of moisture properties of hardened cement pastes, showing hysteresis effects (in French), Mater. Struct. 30 (200) (1997) 340–348.
[22] B. Kari, B. Perrin, J.C. Foures, Vapour permeability of building materials: numerical computation (in French), Mater. Struct. 24 (1991) 227–233.
[23] G. Villain, V. Baroghel-Bouny, J.F. Bouteloup, Assessment of water vapour diffusion coefficient in carbonated and non-carbonated concretes (in French), Proc. of Journées "Durabilité 2006", May 15–16 2006, Paris, France.
[24] S. Hoskova, V. Vydra, Measuring the diffusion coefficient of water vapour permeability, Acta Polytech. 39 (3) (1999) 33–38.
[25] M. Jooss, H.W. Reinhardt, Permeability and diffusivity of concrete as function of temperature, Cem. Concr. Res. 32 (2002) 1497–1504.
[26] R.J. Millington, Gas diffusion in porous media, Science 130 (1959) 100–102.
[27] V.G. Papadakis, C.G. Vayenas, M.N. Fardis, Physical and chemical characteristics affecting the durability of concrete, ACI Mater. J. 88 (2) (1991) 186–196.
[28] J. Sercombe, R. Vidal, F. Adenot, Gas diffusion in cements — Mechanisms and main parameters (in French), Proc. of Colloque National sur les Propriétés de transfert dans les géomatériaux "Transfert 2006", Villeneuve d'Ascq, France, feb. 1–2 2006.
[29] M. Thiery, P. Dangla, G. Villain, G. Platret, E. Massieu, M. Druon, V. Baroghel-Bouny, Modelling the atmospheric carbonation of cementitious materials, Bull. Lab. Ponts Chaussées 252–253 (2004) 153–187.
[30] J.P. Monlouis-Bonnaire, Numerical modelling of coupled air–water–salt transfers in cementitious materials and terracotta (in French), Ph.D. Dissertation, Toulouse, 2003, 213 pp.
[31] A.J. Katz, A.H. Thompson, Quantitative prediction of permeability in porous rock, Phys. Rev., B 34 (11) (1986) 8179–8181.
[32] A.H. Thompson, A.J. Katz, C.E. Krohn, The microgeometry and transport properties of sedimentary rocks, Adv. Phys. 36 (5) (1987) 625–693.
[33] E.J. Garboczi, Permeability, diffusivity and microstructural parameters: a critical review, Cem. Concr. Res. 20 (4) (1990) 591–601.
[34] A.S. EL-Dieb, R.D. Hooton, Evaluation of the Katz–Thompson model for estimating the water permeability of cement-based materials from mercury intrusion porosimetry data, Cem. Concr. Res. 24 (3) (1994) 443–455.
[35] P. Halamickova, R.J. Detwiler, D.P. Bentz, E.J. Garboczi, Water permeability and chloride ion diffusion in portland cement mortars: relationship to sand content and critical pore diameter, Cem. Concr. Res. 25 (4) (1995) 790–802.
[36] P.J. Tumidajski, B. Lin, On the validity of the Katz–Thompson equation for permeabilities in concrete, Cem. Concr. Res. 28 (5) (1998) 643–647.
[37] B.J. Christensen, T.O. Mason, H.M. Jennings, Comparison of measured and calculated permeabilites for hardened cement pastes, Cem. Concr. Res. 26 (9) (1996) 1325–1334.
[38] N.S. Martys, Survey of Concrete Transport Properties and Their Measurement, NIST Report NISTIR, vol. 5592, 1995 40 pp.
[39] D. Perraton, P.C. Aïtcin, A. Carles-Gibergues, Permeability, as seen by the researcher, in: Y. Malier, F.N. Spon (Eds.), High Performance Concrete — From Material to Structure, Chapman and Hall, Cambridge, UK, 1992, pp. 252–275.
[40] V. Baroghel-Bouny, et al., Concrete design for structures with predefined service life — durability control with respect to reinforcement corrosion and alkali–silica reaction, State-of-the-Art and Guide for the Implementation of a Performance-Type and Predictive Approach Based Upon Durability Indicators, Documents Scientifiques and Techniques de l'AFGC, AFGC, Bagneux, july 2004, 252 pp.
[41] N. Hearn, R.H. Mills, A simple permeameter for water or gas flow, Cem. Concr. Res. 21 (2/3) (1991) 257–261.
[42] A.S. El-Dieb, R.D. Hooton, A high pressure triaxial cell with improved measurement sensitivity for saturated water permeability of high performance concrete, Cem. Concr. Res. 24 (5) (1994) 854–862.
[43] G.W. Scherer, Bending of gel beams: method for characterizing elastic properties and permeability, J. Non-Cryst. Solids 142 (1992) 18–35.
[44] W. Vichit-Vadakan, G.W. Scherer, Measuring permeability of rigid materials by a beam-bending method: III — cement paste, J. Am. Ceram. Soc. 85 (6) (2002) 1537–1544.
[45] H. Ai, J.F. Young, G.W. Scherer, Thermal expansion kinetics: method to measure permeability of cementitious materials: II — application to hardened cement paste, J. Am. Ceram. Soc. 84 (2) (2001) 385–391.
[46] G.W. Scherer, Characterization of saturated porous bodies, Mater. Struct. Concr. Sci. Eng. 37 (265) (2004) 21–30.
[47] O. Coussy, V. Baroghel-Bouny, P. Dangla, M. Mainguy, Assessment of the water permeability of concretes from their mass loss during drying (in French), in: V. Baroghel-Bouny (Ed.), Transferts dans les bétons et durabilité, Special issue of Revue Française de Génie Civil, vol. 5, Hermès Science Publications, Paris, 2001, pp. 269–284, n° 2–3.
[48] V. Baroghel-Bouny, M. Mainguy, O. Coussy, Isothermal drying process in weakly permeable cementitious materials — assessment of water permeability, in 'Materials science of concrete', Special volume: 'Ion and mass transport in cement-based materials' (Ed. by R.D. Hooton, M.D.A. Thomas, J. Marchand and J.J. Beaudoin, Series Ed. J.P. Skalny, American Ceramic Society, 2001), pp 59–80.
[49] V. Baroghel-Bouny, M. Thiery, F. Barberon, O. Coussy, G. Villain, Assessment of transport properties of cementitious materials: a major challenge as regards durability?, accepted for publication in Revue Européenne de Génie Civil.
[50] V. Baroghel-Bouny, M. Mainguy, T. Lassabatere, O. Coussy, Characterization and identification of equilibrium and transfer moisture properties for ordinary and high-performance cementitious materials, Cem. Concr. Res. 29 (1999) 1225–1238.
[51] M.Th. van Genuchten, A closed-form equation for predicting the hydraulic conductivity of unsaturated soils, Soil Sci. Soc. Am. 44 (1980) 892–898.
[52] L. Stefan, F. Benboudjema, F. Robert, M. Moranville, Drying and shrinkage — influence of induced cracking (in French), Proc. of Colloque

National sur les Propriétés de transfert dans les géomatériaux “Transfert 2006”, Villeneuve d’Ascq, France, feb. 1–2, 2006.
[53] Y. Mualem, A new model for predicting the hydraulic conductivity of unsaturated porous media, Water Resour. Res. 12 (1976) 513–522.
[54] B.M. Savage, D.J. Janssen, Soil physics principles validated for use in predicting unsaturated moisture movement in portland cement concrete, ACI Mater. J. 94 (1) (1997) 63–70.
[55] N. Bourneton, Estimation of the moisture transport properties of cementitious materials from inverse analyses of laboratory tests (in French), ENTPE-LCPC Report, 2006 57 pp.
[56] H. Looseveldt, Z. Lafhaj, F. Skoczylas, Experimental study of gas and liquid permeability of a mortar, Cem. Concr. Res. 32 (2002) 1357–1363.
[57] I. Yurtdas, N. Burlion, F. Skoczylas, Creep-induced microcracking: effects on the permeability of a mortar submitted to drying (in French), Proc. of Colloque National sur les Propriétés de transfert dans les géomatériaux “Transfert 2006”, Villeneuve d’Ascq, France, feb. 1–2, 2006.
[58] G. Meschke, S. Grasberger, Numerical modeling of coupled hygromechanical degradation of cementitious materials, J. Eng. Mech. 129 (4) (2003) 383–392.
[59] J.J. Kollek, The determination of the permeability of concrete to oxygen by the Cembureau method — a recommendation, Mater. Struct. 22 (1989) 225–230.
[60] Recommended test methods for measuring the parameters associated to durability (in French), Proc. of Journées Techniques AFPC-AFREM “Durabilité des Bétons”, dec. 11–12, 1997, Toulouse, France, LMDC, Toulouse, 1998.
[61] L.J. Klinkenberg, The Permeability of Porous Media to Liquids and Gases, in Drilling and Production Practice, American Petroleum Institute, New York, 1941, pp. 200–213.
[62] P.B. Bamforth, The relationship between permeability coefficients for concrete obtained using liquid and gas, Mag. Concr. Res. 39 (138) (1987) 3–11.
[63] D. Perraton, P.C. Aïtcin., A. Carles-Gibergues, Measurement of gas permeability of concretes: apparent permeability and intrinsic permeability — Part I: validation of Carman’s and Klinkenberg’s concepts in the case of a HPC, Bull. Lab. Ponts Chaussées 221 (1999) 69–78.
[64] A. Abbas, M. Carcasses, J.P. Ollivier, Gas permeability of concrete in relation to its degree of saturation, Mater. Struct. 32 (1999) 3–8.
[65] G. Villain, V. Baroghel-Bouny, C. Kounkou, C. Hua, Gas permeability measurement as a function of the saturation rate of concretes (in French), in: V. Baroghel-Bouny (Ed.), Transferts dans les bétons et durabilité, Special issue of Revue Française de Génie Civil, vol. 5, Hermès Science Publications, Paris, 2001, pp. 251–268, n° 2–3.
[66] F. Jacobs, Permeability to gas of partially saturated concrete, Mag. Concr. Res. 50 (2) (1998) 115–121.
[67] J.C. Parker, R.J. Lenhard, T. Kuppusamy, A parametric model for constitutive properties governing multiphase flow in porous media, Water Resour. Res. 23 (4) (1987) 618–624.
[68] L. Luckner, M.Th. van Genuchten, D.R. Nielsen, A consistent set of parametric models for the two-phase-flow of immiscible fluids in the subsurface, Water Resour. Res. 25 (10) (1989) 2187–2193.
[69] J. Gross, G.W. Scherer, Dynamic pressurization: novel method for measuring fluid permeability, J. Non-cryst. Solids 325 (2003) 34–47.
[70] N. Hearn, Self-sealing, autogenous healing and continued hydration: what is the difference? Mater. Struct. 31 (212) (1998) 563–567.
[71] C. Edvardsen, Water permeability and autogenous healing of cracks in concrete, ACI Mater. J. 96 (4) (1999) 448–454.
[72] N. Hearn, R.J. Detwiler, C. Sframeli, Water permeability and microstructure of three old concretes, Cem. Concr. Res. 24 (4) (1994) 633–640.